Combustion and Flame 158 (2011) 1193–1200

Contents lists available at ScienceDirect

Combustion and Flame

journal homepage: www.elsevier.com/locate/combustflame

Experimental studies on the three-dimensional effects of opposed-flow flame spread over thin solid materials

Xia Zhang [a,*], Yong Yu [b]

[a] Key Laboratory of Microgravity (National Microgravity Laboratory), Institute of Mechanics, Chinese Academy of Sciences, 15 Beisihuanxi Road, Beijing 100190, PR China
[b] School of Aerospace, Beijing Institute of Technology, Beijing 100081, PR China

ARTICLE INFO

Article history:
Received 3 March 2010
Received in revised form 3 August 2010
Accepted 7 October 2010
Available online 2 November 2010

Keywords:
Opposed-flow flame spread
Three-dimensional effect
Thin solid material
Narrow-channel

ABSTRACT

The three-dimensional effects of flame spread over thin solid materials were experimentally studied using a natural-convection-suppressing horizontal narrow-channel. In a sufficiently wide narrow-channel, the variation of flame spread against the width of the material sample showed different trends for different gas flow speeds and oxygen concentrations. The extent of three-dimensional effects was inversely proportional to the gas flow speed or its square. Near quenching extinction limits, the effects were significant because weak combustion is sensitive to a slight variation of heat loss and oxygen concentration. The effects may be due to different factors such as side heat loss, side oxygen diffusion, or both. Far away from quenching extinction limits, the effects were weak because vigorous combustion is insensitive to a small variation of oxygen concentration and heat loss. In all tests, the effects were limited to the samples of width less than 10 times of the diffusion length. Moreover, a higher oxygen concentration suppressed the effects at a lower gas flow speed. For sufficiently wide samples, in the most range of gas flow speeds, the channel width had almost no effect on flame spread. However, near extinction limits, the flame spread rate decreased with the increasing channel width.

1. Introduction

Material flammability is a critical index used in excluding potential fuels from materials used in manned spacecraft to ensure fire safety [1]. Microgravity tests provide a basis for material flammability assessment. Flame spread tests are important in making the assessment. However, in microgravity tests performed in drop towers or aboard spacecraft or microgravity airplanes, the geometrical sizes of test sections, gas flow rates, and material samples are usually small due to limited conditions. Therefore, it is difficult to realize two-dimensional flame spread tests in microgravity. Meanwhile, in facilities both on the ground and aboard spacecraft, not all materials in actual use are sufficiently wide. Nonetheless, the sizes of flow tunnels and materials will certainly influence flame spread. Consequently, the three-dimensional effects must be considered for both the good interpretation of test results and the exact prediction of material flammability.

Previous studies on the three-dimensional effects of flame spread over solid materials have involved the experimental investigations of opposed-flow flame spread in the buoyantly convective environment of normal and high gravity [2–4] and the numerical simulations of opposed-flow and concurrent-flow flame spread in the low-speed forced flow environment of microgravity [5–8]. These studies were all conducted for thin solid materials. Sibulkin et al. [2] experimentally showed that in the buoyantly convective environment of normal gravity, the downward flame spread rate rises with the increasing sample width, until the width reaches 2 cm at which the flame spread rate arrives at its asymptotic value. This result was supported by Frey and T'ien's experiments [3] for downward flame spread in normal gravity environment of 20.7 kPa and 68.9 kPa. Frey and T'ien's experiments implied that near extinction limits, a small variation of the sample width may strongly influence the flame spread rate. In Altenkirch et al.'s experiments with various pressures and gravity levels (1.0–8.0 g) [4], the downward flame spread rate was observed to be independent of the sample width when it is wider than 1.3 cm. Although it has been believed that the flame spread rate increases with the widening sample is caused by decreased heat loss, more parameters are still necessary to be taken into account.

The three-dimensional effects of flame spread in low-speed gas flows are investigated recently. Mell and Kashiwagi numerically compared two-dimensional and three-dimensional transitions from ignition to flame spread and subsequent flame spread in the forced flows of flow speed less than 12 cm/s [5,6]. It was found that a three-dimensional flame with a narrow width develops more easily than a two-dimensional flame due to additional oxygen diffusion from the lateral sides of the three-dimensional flame. In addition, for opposed-flow flame spread, the effects of

* Corresponding author. Fax: +86 10 62525301.
E-mail address: dr.xiazhang@gmail.com (X. Zhang).

0010-2180/$ - see front matter © 2010 The Combustion Institute. Published by Elsevier Inc. All rights reserved.
doi:10.1016/j.combustflame.2010.10.004

Nomenclature

B	pre-exponential factor of reaction
Cp	specific heat
D	mass diffusivity
E	activation energy
ΔH	reaction heat
L	length scale
Le	Lewis number
R	universal gas constant, ratio
T	temperature
u	velocity
W	width
x, y, z	coordinates
Y	mass fraction
α	thermal diffusivity
λ	thermal conductivity
ρ	density

Subscripts and superscripts

$'$	dimensionless quantity
c	channel
f	flame or combustible material sample
g	gas
O	oxygen
r	reference value, radiative
x, y, z	coordinates
∞	ambience

the sample width on the flame are more significant in lower speed gas flows. In this case, the flame spread rate over a narrower sample is higher, since side oxygen diffusion relieves the impediment imposed by expansion-induced velocity for oxygen to enter into the reaction region, while the increase of the gas flow speed weakens the effects. These findings indicated another aspect of three-dimensional effects of flame spread. Shih and T'ien [7,8] and T'ien et al. [9] performed three-dimensional numerical simulations for concurrent-flow flame spread and further confirmed two aspects of three-dimensional effects: one is dominated by side heat loss and the other is by side oxygen diffusion. The former occurs when a flame is under conditions far away from its quenching extinction limit, in which case, a wider sample has a quicker flame spread rate and a wider flammability limit. This is in agreement with the above-mentioned experimental results. While the latter happens when a flame is under conditions near the quenching extinction limit where oxygen supply controls the flame, in which case, a narrower sample has a quicker flame spread rate and a wider flammability limit.

To sum up, the influences of many factors on the three-dimensional effects of flame spread remain to be studied experimentally, and numerical simulation results remain to be validated. In addition, no research has been done for the whole range of gas flow speeds including regions near quenching and blow-off extinction limits and the thermal region. The present paper presents our systematic experimental studies on three-dimensional effects of flame spread over thin solid materials, considering parameters such as gas flow speed, oxygen concentration, material width, and flow tunnel size. To avoid the interference of natural convection on flame spread, the experiments used a natural-convection-suppressing horizontal narrow-channel. Such a facility has been used in the research of fingering instability in solid fuel combustion to suppress the natural convection by Zik and Moses [10], and of polymer material combustion to simulate microgravity by Ivanov et al. [11] and Melikhov et al. [12]. Olson et al.'s results on finger-like smoldering in microgravity [13] and Zhang's results on flame spread [14,15] over thin solid materials in normal and microgravity confirmed that the device can suppress natural convection effectively and simulate microgravity. Experimental results in Section 3.3 of this paper also showed the natural-convection-suppressing property of the device.

2. Experiments

As shown in Fig. 1, the experimental system consisted of a test section, a gas supply subsystem, and an image record and analysis

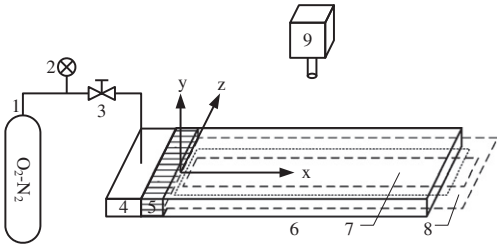

Fig. 1. Experimental system. The test section in this figure was a natural-convection-suppressing horizontal narrow-channel with a length of 70 cm, a height of 10 mm, and an adjustable width in the range of 12–24 cm. (1) O_2–N_2 gas bottle, (2) flowmeter, (3) valve, (4) gas inlet chamber, (5) aluminum honeycomb, (6) combustion chamber, (7) fuel sample, (8) sample frame, (9) camera.

subsystem. The test section was a natural-convection-suppressing horizontal narrow-channel, whose inlet was filled with aluminum honeycomb to ensure a uniform gas flow. The channel had a length of 70 cm, a height of 10 mm, and an adjustable width W_c in the range of 12–24 cm, which was at least 12 times as its height so that a two-dimensional flow was achieved in its central section. For the convenience of observation, channel walls were made of glass with the surface facing the camera being covered with transparent film printed with 1 cm grids as a ruler. The sample frame was symmetric and made of aluminum alloy with a thickness of 1 mm, a length of 70 cm, and an outer width the same as the channel width. During experiments, the sample frames with different inner widths from 1 cm to 12 cm were used to match the combustible sample width or the flame width W_f (which will be called the sample width for brevity in the following). The gas supply subsystem consisted of a gas bottle charged with a mixture of oxygen and nitrogen, a flowmeter, and connecting pipelines. A glass rotor flowmeter with the maximum scale of 6 m^3/h and two mass flow controllers with the maximum scales of 20 l/min and 5 l/min were used to measure the flow rates of the gas at high levels (above 20 l/min), middle levels (20–5 l/min), and low levels (below 5 l/min), respectively, to obtain both good precision and wide measurement range. The mass flow controllers also controlled the flow rates. The image record and analysis subsystem consisted of a Sony DCR-TRV900E Digital Video Camera Recorder with a resolution of 450,000 pixels to record flame images at a speed of 25 frames per second and a PC computer (not shown in Fig. 1) to analyze the recorded images.

The experimental procedure was as follows: a sample was attached onto a sample frame, which was in turn inserted into the middle of the channel with an equal distance to the top and bottom walls of the channel. Then an O_2–N_2 gas mixture flow with a

specific and adjustable flow rate was started with the camera being turned on at the same time. Next, the sample was ignited with an electrically heating wire from the end of the channel outlet. After experiments, the flame images recorded by the camera were transferred into a computer for further analysis.

The coordinate system was established with the center of the inlet of the channel as the origin. Numerical simulations considering the fuel presence but no burning showed that the gas flows were in fully developed or near fully developed conditions when $x > 40$ cm (Reynolds numbers were from 3.3 to 200 if the half height of the channel was used as the length scale); while the analysis of flame images showed that the flame spread was approximately in a steady state when $x < 60$ cm. Therefore, flame spread rates were calculated according to the propagating distances of the centerline leading edges of the flames in the range of 40 cm $< x <$ 60 cm as a function of time. Since the purpose of the present paper is to study steadily spreading flames, only those flames with a continuous leading edge were calculated while finger-like flamelets were marked but not given a speed. The half height of the channel and the thickness of the top glass wall were only 5 mm and the distance from the lens of the camera to the glass wall was about 80 cm. The difference between sample and glass planes might not affect the calculation results of flame spread rates. This could be indirectly validated by the fact that the lateral sides of flame and scale in Fig. 2 coincided with each other. Therefore, the difference was not taken into account when flame spread rates were calculated.

The O_2–N_2 gas mixtures used in the experiments were commercially prepared with the oxygen mass fractions Y_o of 20.0%, 23.3%, and 32.9% (the corresponding volume fractions of 18.0%, 21.0%, and 30.0%), respectively. The sample was copy paper with a thickness of 0.0245 mm and an area density of 17.0 g/m^2. Based on flow rates and the section area of the channel, the average gas flow speed u was in the range of 1–50 cm/s. The ambient temperature during the experiments was 20 °C.

The relative errors of variables were estimated as follows: the oxygen concentration ±1%, the area density ±6%, the height of the channel ±2%, the channel width ±2%, and the sample width ±2%. The calculated error of the flame spread rate due to the ambiguity of the leading edge of the flame was 4%, and that due to the difference between the planes of grids and sample was 1.5%.

The glass rotor flowmeter had the maximum absolute error of 6 m^3/h × 2.5% = 2.5 l/min, corresponding to the maximum relative error of 11.6% at 21.6 l/min (15.0 cm/s). The mass flow controller with the maximum scale of 20 l/min had the maximum absolute error 20 l/min × 2% = 0.4 l/min, corresponding to the maximum relative error of 5.6% at 7.2 l/min (5.0 cm/s). The mass flow controller with the maximum scale of 5 l/min had the maximum absolute error 5 l/min × 2% = 0.1 l/min, corresponding to the maximum relative error of 6.9% at 1.44 l/min (1 cm/s).

3. Results and discussion

3.1. Flame appearance

Flame images for samples of different widths in the gas flows of 23.3% oxygen are shown in Fig. 2. Their x coordinates were from 40 to 45 cm.

In the gas flows of 1 cm/s, the leading edges of flames over samples narrower than 4 cm were continuous and smooth. In contrast, those over samples wider than 4 cm split into two parts or even formed finger-like flamelets during spread, which were also observed in Olson and T'ien's experiments of buoyant low-stretch diffusion flames beneath PMMA columns [16]. This suggests that even if a two-dimensional flame cannot sustain itself, a three-dimensional flame may spread. Such phenomena are critical for the assessment of material flammability and can be explained by the sensitivity of combustion reactions to heat loss and oxygen supply under conditions near the quenching extinction limit. For a narrower sample, more oxygen can diffuse from the lateral sides of the flame and feed into the reaction region to enhance combustion and to smooth the leading edge of the flame. However, the side oxygen diffusion has a maximum diffusion length. Once the half

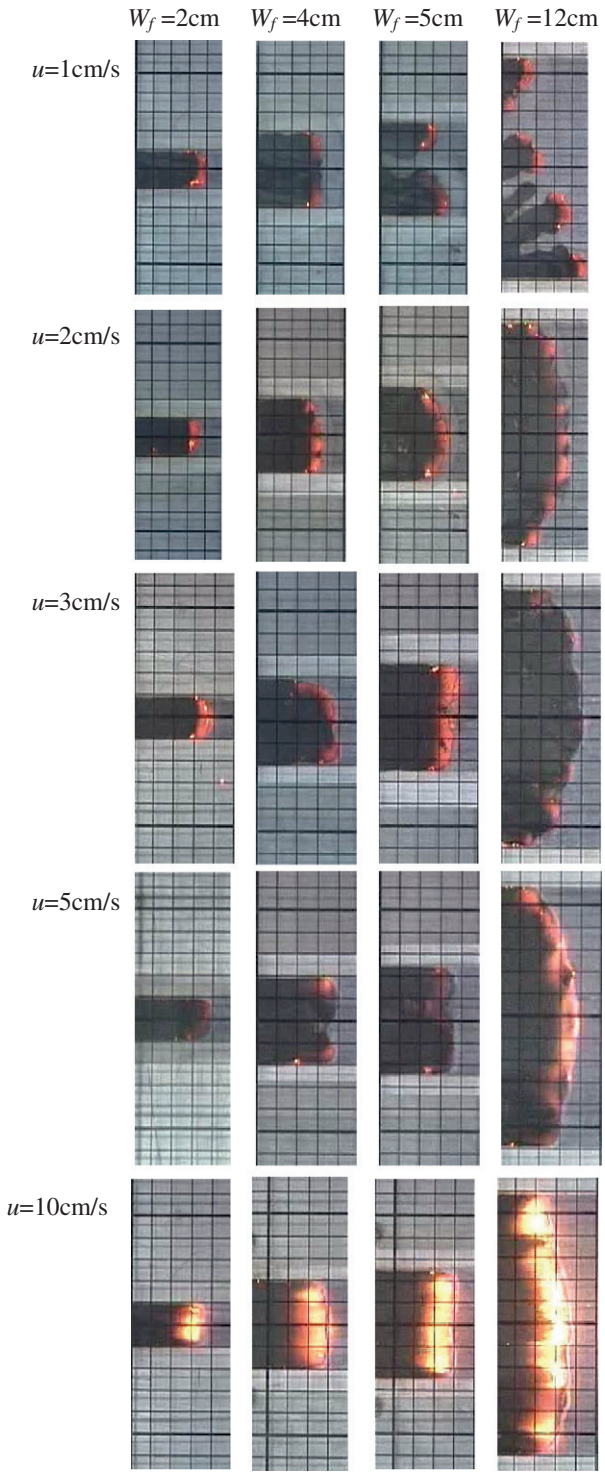

Fig. 2. Flame images for samples of different widths in the gas flows of Y_o = 23.3%. Their x coordinates were from 40 to 45 cm. The length of the grid was 1 cm. The flame propagated from left to right and the gas flowed from right to left.

width of the sample is greater than the maximum length, the side oxygen cannot diffuse into the flame center any more. Therefore, the flame extinguishes or breaks into flamelets due to the shortage of oxygen. This is in agreement with the results of reference [13] that an array of smoldering spots can drive the local oxygen flux between spots to such low levels that smoldering can no longer be sustained in over a substantial fraction of the surface. Dimensional analysis shows that the diffusion length of oxygen can be estimated as $L \sim D/u_r \sim \alpha/u_r \sim \alpha/(u + u_f)$, where D, α, u_r, and u_f are the mass diffusivity, the thermal diffusivity, the reference velocity, and the flame spread rate, respectively. When the reference temperature is taken as 1000 °C, the diffusion length of oxygen, $L \sim 2.46\ \text{cm}^2/\text{s}/1.2\ \text{cm/s} = 2.05\ \text{cm}$, which is in good agreement with the experimental observation.

For the gas flows of 2 cm/s, the leading edges of flames over samples of various widths were continuous. Narrow samples burnt out completely, while for wide samples, due to the existence of local extinction spots, unburnt residues were left behind. This is because the flow rates of 2 cm/s is still very close to the quenching extinction limit and combustion is vulnerable to a minor variation of oxygen supply and heat loss. Consequently, side oxygen diffusion can help narrow samples to burn completely, while heat loss can render all the leading edges of flames in parabola shapes. For the gas flows of 3 cm/s, similar results were also observed. For still higher speed gas flows, wide samples burnt out completely.

Flame images over 12 cm wide samples are shown in Fig. 3. Their x coordinates were from 40 to 45 cm. For 20.0% oxygen, the flames in 1 cm/s and 35 cm/s gas flows could not propagate. For low-speed gas flows, the shape of flames at 20.0% and 32.9% oxygen was similar to that at 23.3% oxygen. In addition, at all three oxygen levels, as the gas flow speed increased, the curvature of the leading edge and the three-dimensional effects of the flame were reduced. Moreover, a higher oxygen concentration suppressed three-dimensional effects at a lower gas flow speed. For example, at $Y_o = 32.9\%$, a gas flow speed higher than 2 cm/s made the leading edge of the flame almost in the form of a straight line except for local extinction points and margins.

3.2. Variation of flame spread rate against sample width in the narrow-channel of 24 cm wide

The effects of the sample width on the flame spread rate are shown in Fig. 4. Repeat tests were done for the extremely low speed gas flows to confirm the flamelets. For the fuel width of 5 cm, in the lowest speed gas flows, all of the flames broke up into flamelets during their propagation from $x = 40$ cm to $x = 60$ cm. Vertical dotted lines were used to mark such cases. However, for the fuel width of 4 cm, some flames broke up into flamelets, but others propagated with a continuous flame edge. For such cases, the flame spread rates were not explicitly given. Wider widths than the sample width showing flamelets were not tested. The purpose of this paper is to study steadily spreading flame. Interesting discussions on flamelet phenomena in flame spread were given by Olson et al. [17].

At all three oxygen levels, as gas flow speeds were higher than 10 cm/s, three-dimensional effects were weak. In addition, for samples wider than 2 cm, flame spread rates approached their asymptotic values, which is in good agreement with the previous results [2–4]. Moreover, for samples with a 12 cm width, regardless of the gas flow speed, the flame spread rate approached an asymptotic value rather than depended on the sample width. This result has not been reported elsewhere previously, to the author's knowledge.

For gas flows with $Y_o = 23.3\%$ (Fig. 4b), near the quenching extinction limit, three-dimensional effects strongly affected flame spread. The variation of the flame spread rate against the sample

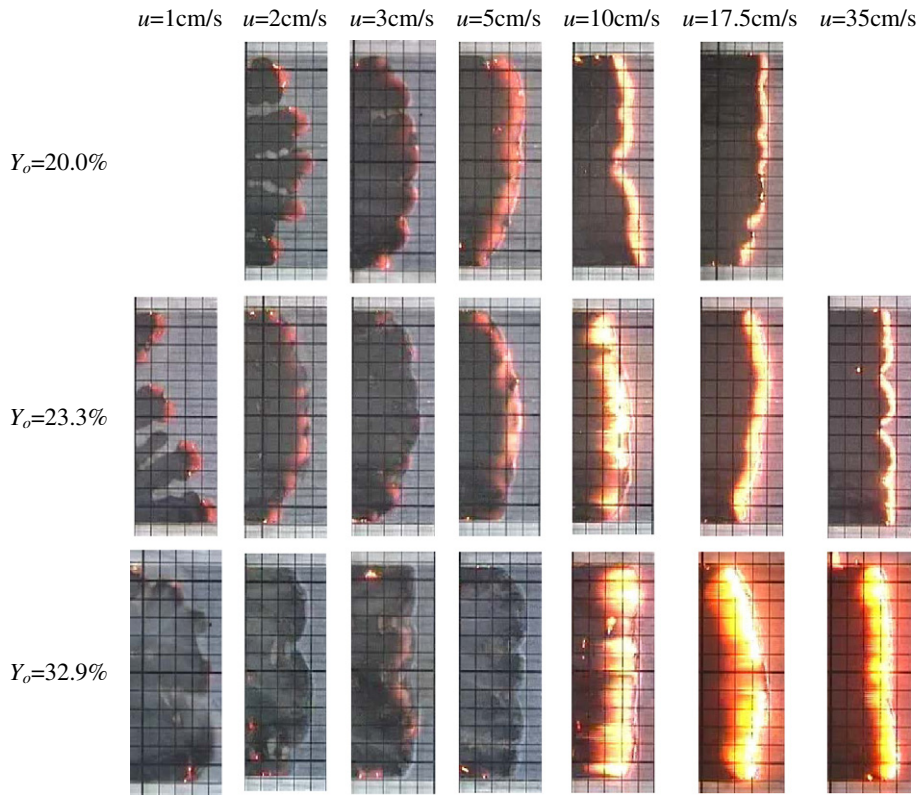

Fig. 3. Flame images for 12 cm wide samples. Their x coordinates were from 40 to 45 cm. The length of the grid was 1 cm. For 20.0% oxygen, the flames in 1 cm/s and 35 cm/s gas flows could not propagate.

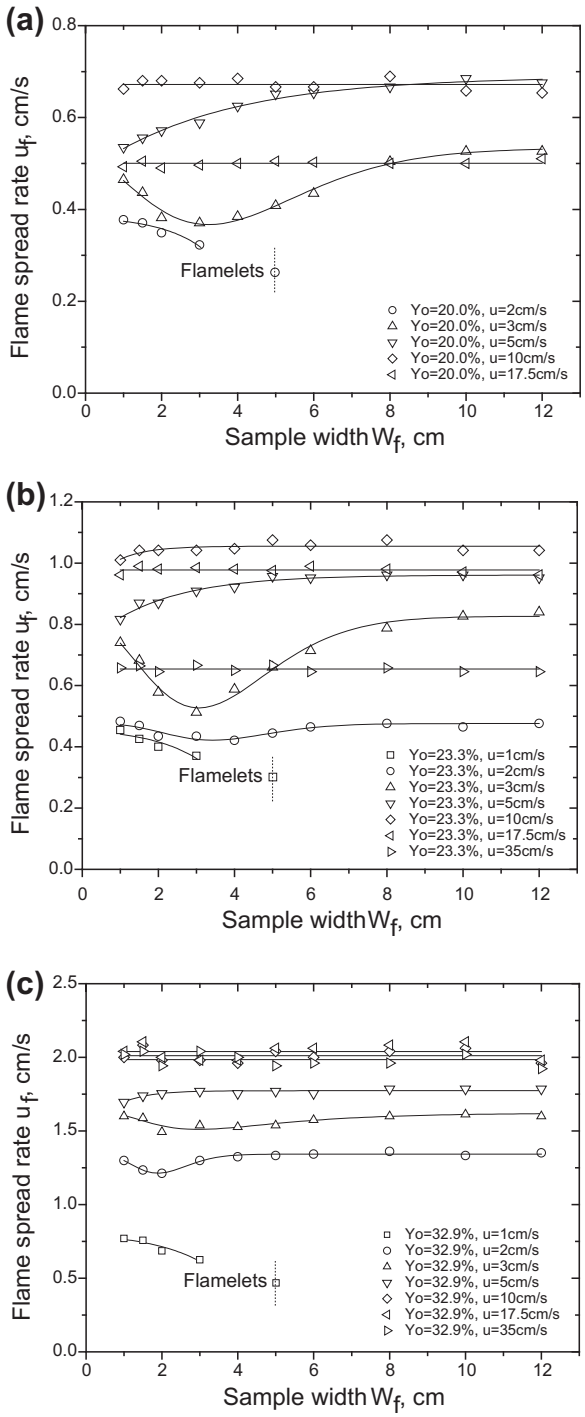

Fig. 4. The flame spread rate as a function of the sample width: (a) Y_o = 20.0%; (b) Y_o = 23.3%; (c) Y_o = 32.9%.

width took complicated trends. For extremely low speed gas flows (1 cm/s), combustion is short of oxygen. Therefore, the side oxygen diffusion dominated the three-dimensional effects. As a result, as the sample became wider, the side oxygen diffusion decreased and flame spread became slower. For the sample wider than 5 cm, the side oxygen diffusion could not reach the sample center, as shown in Fig. 2.

In slightly higher speed gas flows (3 cm/s), both side oxygen diffusion and heat loss significantly influenced the flame spread, resulting in a complicated variation trend of the flame spread rate against the sample width. The side oxygen diffusion still prevailed over the side heat loss. As the sample got wider, the side oxygen diffusion became weaker and the flame spread rate decreased. However, when the sample width exceeded a critical value, the side oxygen diffusion could not reach the center of the sample. After that, with a further increase of the sample width, the side heat loss would dominate three-dimensional effects. As a result, as the sample became wider, the side heat loss decreased while the flame spread rate increased. The minimum flame spread rate appeared for the samples of 3 cm wide. This is in agreement with Fig. 2 and the oxygen diffusion length proposed by both previous [7] and present analyses.

In higher speed gas flows (5 cm/s) the flame is under conditions slightly further away from the quenching extinction limit, and the effects of the side heat loss prevailed over those of the side oxygen diffusion. Therefore, the flame spread rate increased as the sample got wider.

For even higher speed gas flows (over 10 cm/s), the flame spread will be in the thermal region, where oxygen is plentiful, the opposed flows are not excessive, and chemical kinetics are sufficiently fast so that the flame spread is dominated by thermal conduction in the gas phase. The flame spread will be less influenced by the sample width. Only for very narrow samples, the sample width affected the flame spread rate. As the gas flow speed further increases (to 17.5 cm/s or over), the flame enters the near blow-off limit region, the three-dimensional effects were decreased, and the flame spread rate became almost independent of the sample width.

At decreased (Fig. 4a) or increased (Fig. 4c) oxygen concentrations, in every region of flame spread including regions near quenching and blow-off extinction limits and thermal regions, the variation of the flame spread rate against the sample width showed the same trend as in the same flame spread region at Y_o = 23.3%. In addition, weaker three-dimensional effects at higher oxygen concentration could be identified. This is mainly because the flame is under conditions far away from the extinction limit and the vigorous reaction is not sensitive to a small variation of oxygen supply and heat loss.

The dimensionless form of data in Fig. 4 is shown in Fig. 5, where the sample width W_f and the flame spread rate u_f are scaled by L, the diffusion length, and $u_{f,\max}$, the maximum value of the flame spread rates at the same gas flow speed, respectively. For all oxygen concentrations and gas flow speeds, the three-dimensional effects of the flame spread were restricted in the range of the dimensionless sample width $W_f/L < 10$. Above this value, the flame spread rate would cease to change with the width. For the

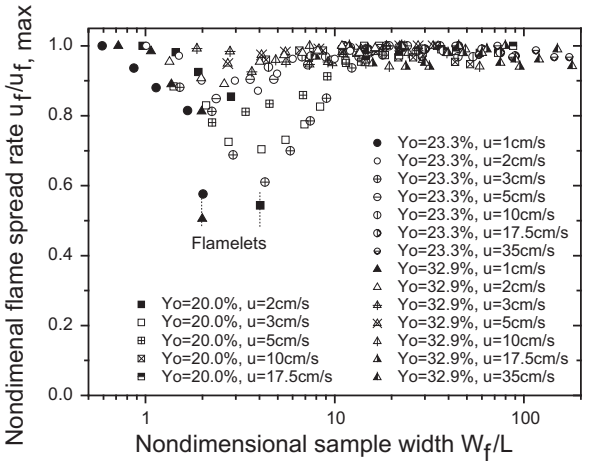

Fig. 5. The dimensionless flame spread rate as a function of the dimensionless sample width. The sample width W_f and the flame spread rate u_f are scaled by L, the diffusion length, and $u_{f,\max}$, the maximum value of the flame spread rates at the same gas flow speed, respectively.

gas flow speeds of 2 cm/s and 10 cm/s, the critical sample widths were 12 cm and 2.5 cm, respectively. In addition, at higher oxygen concentration (Y_o = 32.9%), combustion is vigorous and is not sensitive to a minor alteration of oxygen supply and heat loss. Therefore, when the dimensionless sample width was greater than 4, the flame spread rate was not affected by the three-dimensional effects any more (for the gas flow speeds of 2 cm/s and 10 cm/s, the critical sample widths were 5 cm and 1 cm, respectively.). However, at lower oxygen concentrations (Y_o = 20.0% or 23.3%), near the quenching extinction limit (u = 3 cm/s or 5 cm/s), when the dimensionless sample width approached 4, the flame spread rate approached its minimum value.

In order to analyze the three-dimensional effects in a simple way, an energy and oxygen balance model for the leading edge of the flame with the dimensions of L_x, L_y, and L_z was developed, which considers the input, output, and change of energy and oxygen in a control volume containing the leading edge of the flame. It can be written as

$$\Delta H B\rho^2 Y_f Y_{of} e^{-E/RT_f} L_x L_y L_z = \rho u C_p (T_f - T_\infty) L_y L_z + \frac{(\lambda+\lambda_r)(T_f - T_\infty) L_y L_z}{L_x} + \frac{2(\lambda+\lambda_r)(T_f - T_\infty) L_x L_z}{L_y} + \frac{2(\lambda+\lambda_r)(T_f - T_\infty) L_x L_y}{L_z} \quad (1)$$

$$-B\rho Y_f Y_{of} e^{-E/RT_f} L_x L_y L_z = u(Y_{of} - Y_{o\infty}) L_y L_z + \frac{\alpha(Y_{of} - Y_{o\infty}) L_y L_z}{LeL_x} + \frac{2\alpha(Y_{of} - Y_{o\infty}) L_x L_z}{LeL_y} + \frac{2\alpha(Y_{of} - Y_{o\infty}) L_x L_y}{LeL_z} \quad (2)$$

where ρ, T, Y_f, λ, λ_r, Cp, ΔH, B, E, R, and Le are the gas density, the temperature, the fuel mass fraction, the thermal conductivity, the radiative conductivity, the specific heat, the reaction heat, the pre-exponential factor of reaction, the activation energy, the universal gas constant, and the Lewis number, respectively. The terms in Eqs. (1) and (2) are reaction source or sink, convection, and diffusion in x, y, and z directions. The diffusion terms in z direction reflect three-dimensional effects. For the heat balance equation, the heat radiation is treated in the form of conduction for simplification.

The variation of three-dimensional effects with the gas flow speed may be evaluated according to the ratio of lateral diffusion term to convection term, i.e.,

$$R_{3d,T} = 2(\alpha+\alpha_r)L_x/uL_z^2 \quad (3)$$

for heat and

$$R_{3d,O} = 2\alpha L_x/uLeL_z^2 \quad (4)$$

for oxygen. Evidently, the three-dimensional effects are inversely proportional to the square of the length scale in z direction, and to the gas flow speed if L_x is independent of the gas flow speed, or to the square of the gas flow speed if $L_x \sim 1/u$. This indicates three-dimensional effects will become strong as the gas flow speed or fuel width decreases. These results are in good agreement with the experimental results.

In extremely low speed gas flows, the flame is near the quenching extinction limit and its leading edge is short of oxygen supply [18]. Therefore, the effects of oxygen supply on the flame surpass those of temperature. The flame spread rate will decrease as the fuel becomes wider, which is in contrary with the cases far away from the quenching extinction limit. Meanwhile, mass diffusion has a shorter length scale than heat transfer. As a result, the flame spread rate increases with the increasing fuel width, if the fuel width has surpassed a critical value. This may be the reason why there was a minimum in the flame spread rate as a function of the fuel width. The above analysis is also supported by the fact that the width corresponding to the minimum was just about twice the flamelet width and that the flamelets started at just above this width (Figs. 2 and 3), where the two-dimensional flame could no longer survive, and the flame broke up into flamelets.In the diffusion flame, Y_{of} is much smaller than $Y_{O\infty}$, and Eq. (2) can be simplified as

$$B\rho Y_f Y_{of} e^{-E/RT_f} L_x L_y L_z = uY_{o\infty} L_y L_z + \frac{\alpha Y_{o\infty} L_y L_z}{LeL_x} + \frac{2\alpha Y_{o\infty} L_x L_z}{LeL_y} + \frac{2\alpha Y_{o\infty} L_x L_y}{LeL_z} \quad (5)$$

This shows that the oxygen concentration and side oxygen diffusion at the leading edge of the flame is proportional to its ambient value. Therefore, high oxygen ambient will result in high oxygen concentration at the leading edge of the flame and hence can relieve the oxygen shortage and suppress three-dimensional effects more easily than low oxygen ambient. In cases far away from the quenching extinction limit, the relative importance of three-dimensional effects due to heat loss and mass diffusion may be proportional to the ratio of $R_{3d,T}$ and $R_{3d,O}$ i.e., $Le(\alpha+\alpha_r)/\alpha$. If Le is unity and radiative heat transfer is ignored, then the three-dimensional effects caused by lateral heat loss and mass diffusion will counterbalance each other. However, if radiative heat transfer is considered, or Lewis number is not unity, or both (for oxygen, Le is a number slightly greater than 1), there will be three-dimensional effects since the ratio will be greater than 1. In this case, the three-dimensional effects due to heat loss will surpass those due to mass diffusion and the flame spread rate will increase as the fuel becomes wider.

Mell and Kashiwagi's modeling [6] showed that for both 2 cm/s and 10 cm/s gas flows, the flame spread rates decrease with the increase of the sample widths. For narrow samples and low speed gas flows the present experiments and M&K's modeling results are qualitatively agreed. However, for wide samples or high-speed gas flows, the trends of the present experimental results, i.e., the flame spread rates increased with the increase of the sample widths, and the M&K's modeling results are completely different. This may be attributed to the fact that M&K modeled flame spread in the oxygen-limited regime and the radiative heat loss of gas phase was ignored. The modeling considering more complicated factors such as different gas flow speeds and oxygen concentra-

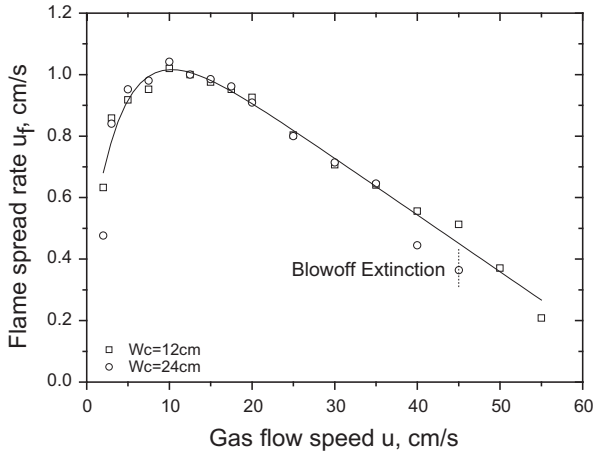

Fig. 6. Flame spread rates for 12 cm wide samples in channels of 12 cm and 24 cm in width (Y_o = 23.3%).

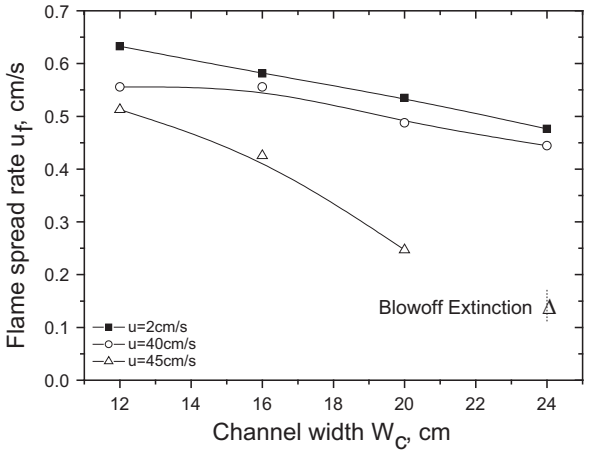

Fig. 7. The flame spread rate for 12 cm wide samples as a function of the channel width (Y_o = 23.3%).

tions, and radiative heat loss may reproduce the results of the present paper.

3.3. Variation of flame spread rate over 12 cm wide samples against channel width

The flame spread rates for 12 cm wide samples in channels of 12 and 24 cm in width are illustrated in Fig. 6. The results showed that the flame spread rate first increased and then decreased as the gas flow speed increased. This trend qualitatively reproduced the microgravity experimental results given by reference [18] and implied that the horizontal narrow-channel can suppress buoyant convection effectively. For a great part of gas flow speeds, the channel width had almost no effect on the flame spread rate. However, near extinction limits, the flame spread rate was obviously affected by the channel width.

The effects of channel width on the flame spread rate near extinction limits are shown in Fig. 7. Near both quenching and blow-off extinction limits, the flame spread rate decreased with the channel width. This can be explained as follows: near the quenching extinction limit, as the channel becomes wider, the gas flow becomes easier to divert around the flame, resulting in a lower opposed-flow velocity at the flame front and hence a lower flame spread rate. This explanation can obtain an indirect support from Mell and Kashiwagi's numerical results [6] of transition and flame spread in microgravity that the velocity due to thermal expansion from the flame reduces the net inflow of oxygen to affect flame behavior. By contrast, near the blow-off extinction limit, as the channel becomes wider, the gas flow speeds at the edges of the sample increase due to the farther laminar layers near the side walls, which reduces the flame spread rate and the gas flow speed limit corresponding to the blow-off extinction.

4. Conclusion

The present paper experimentally studies the three-dimensional effects of flame spread over thin solid materials using a natural-convection-suppressing horizontal narrow-channel. The effects of gas flow speed, oxygen concentration, material width, and flow tunnel size on flame spread are considered.

In a sufficiently wide channel, the variation of flame spread against the sample width was different for different gas flow speeds and oxygen concentrations. At low oxygen concentrations, near quenching extinction limits, the three-dimensional effects of flame spread were significant and complicated. In extremely low speed gas flows, side oxygen diffusion dominates the three-dimensional effects. Accordingly, as the sample became wider, side oxygen diffusion decreased and flame spread became slower. Since the side oxygen diffusion has a maximum diffusion length, when the half width of the sample went beyond that maximum length, the leading edge of the flame split into two parts or even formed finger-like flamelets in contrast to the continuous and smooth leading edge of the flame of narrower samples. This indicates that even when a two-dimensional flame ceased to spread, a three-dimensional flame may spread. In slightly higher speed gas flows, both the side oxygen diffusion and heat loss significantly influence the flame spread. As the sample width increased, the flame spread rate first decreased and then increased, depending on whether the side oxygen diffusion or the side heat loss dominated the three-dimensional effects. In addition, a narrower sample could burn out completely, while the flame of a wider sample had local extinction spots, and unburnt residues were left behind. Moreover, heat loss made the leading edges of flames parabola shapes. In higher speed gas flows the flame is in conditions somehow far away from the quenching extinction limit, and the effects of the side heat loss prevail over those of the side oxygen diffusion. Therefore, the flame spread rate increased as the sample became wider. In addition, the curvature of the leading edge and the three-dimensional effects of the flame decreased accordingly. Moreover, the effects of both side heat loss and side oxygen diffusion decreased rapidly with the gas flow speed.

Under conditions far away from the quenching extinction limit, i.e., at high oxygen concentrations or high-speed gas flows, the three-dimensional effects were weaker because a vigorous reaction is not sensitive to a small variation of oxygen supply and heat loss. For all oxygen concentrations and gas flow speeds, the three-dimensional effects of the flame spread were restricted to the samples of width less than 10 times of the diffusion length (for the gas flow speeds of 2 cm/s and 10 cm/s, the critical sample widths were about 12 cm and 2.5 cm, respectively). Moreover, a higher oxygen concentration could suppress three-dimensional effects at a lower gas flow speed.

For a sufficiently wide sample, for a great part of gas flow speeds, the channel width had almost no effect on the flame spread rate. However, near quenching and blow-off extinction limits, the flame spread rate decreased with the increasing channel width.

Due to the disadvantages of the experimental facility such as additional heat loss caused by top and bottom walls, the above conclusions should be further validated under better and simpler experimental conditions such as microgravity. In addition, the results are only of qualitative significance. A quantitative interpretation may be based only on three-dimensional numerical simulations.

Acknowledgments

The author thanks Prof. Wenrui Hu of Institute of Mechanics, Chinese Academy of Sciences for his invaluable advice. This work was supported by Chinese Academy of Sciences (CAS) Innovation Program and National Science Foundation of China (NSFC Grant No. 10702009).

References

[1] R. Friedman, Fire Mater. 20 (1996) 235–243.
[2] M. Sibulkin, W. Ketelhut, S. Feldman, Combust. Sci. Technol. 9 (1974) 75–77.
[3] A.E. Frey Jr., J.S. T'ien, Combust. Flame 26 (1976) 257–267.
[4] R.A. Altenkirch, R. Eichhorn, P.C. Shang, Combust. Flame 37 (1980) 71–83.
[5] W.E. Mell, T. Kashiwagi, Proc. Combust. Inst. 27 (1998) 2635–2641.
[6] W.E. Mell, T. Kashiwagi, Proc. Combust. Inst. 28 (2000) 2785–2792.
[7] H.-Y. Shih, J.S. T'ien, Proc. Combust. Inst. 28 (2000) 2777–2784.
[8] H.-Y. Shih, J.S. T'ien, Combust. Theory Model. 7 (2003) 677–704.

[9] J.S. T'ien, H.-Y. Shih, C.-B. Jiang, H.D. Ross, F.J. Miller, A.C. Fernandez-Pello, J.L. Torero, D.C. Walther, in: H.D. Ross (Ed.), Microgravity Combustion: Fire in Free Fall, Academic Press, San Diego, 2001, pp. 299–418.
[10] O. Zik, E. Moses, Proc. Combust. Inst. 27 (1998) 2815–2820.
[11] A.V. Ivanov, Ye.V. Balashov, T.V. Andreeva, A.S. Melikhov, Experimental Verification of Sample Flammability in Space, Report No. NASA CR-1999-209405, National Aeronautics and Space Administration, 1999.
[12] A.S. Melikhov, I.A. Bolodyan, V.I. Potyakin, A.V. Ivanov, V.F. Alymov, A.B. Smirnov, D.Ye. Belov, Ye.V. Balashov, T.V. Andreeva, in: K. Sacksteder (Ed.), Fifth International Microgravity Combustion Workshop, National Aeronautics and Space Administration, 1999, pp. 361–364 (May 18–20).
[13] S.L. Olson, H.R. Baum, T. Kashiwagi, Proc. Combust. Inst. 27 (1998) 2525–2533.
[14] X. Zhang, J. Jpn. Soc. Microgravity Appl. 24 (2007) 234–240.
[15] X. Zhang, Chin. J. Theory Appl. Mech. 39 (2007) 466–472 (in Chinese).
[16] S.L. Olson, J.S. T'ien, Combust. Flame 121 (2000) 439–452.
[17] S.L. Olson, F.J. Miller, I.S. Wichman, Combust. Theory Model. 10 (2006) 323–347.
[18] S.L. Olson, Combust. Sci. Technol. 76 (1991) 233–249.